LANGMUIR

pubs.acs.org/Langmuir Article

Porous Morphology of High Grafting Density Mixed Polyelectrolyte Brushes Grown from a Y-Inimer Coating

Published as part of Langmuir virtual special issue "Highlights in Interface Science and Engineering: Polymer Brushes".

Julia D. Smith, Ri Chen, Nicolas Noriega Osores, and Padma Gopalan*

Cite This: https://doi.org/10.1021/acs.langmuir.4c00556 Read Online

ACCESS | Metrics & More | Article Recommendations | Supporting Information

ABSTRACT: Mixed A/B polyelectrolyte (PE) brushes of opposite charges are grown from a Y-shaped initiator-bearing coating to facilitate intimate mixing of the A and B polyelectrolytes in a 1:1 grafting ratio. The design of the Y-shaped inimer includes both ATRP and NMP initiators attached to a common Y-junction. A copolymer of a Y-shaped inimer with glycidyl methacrylate is cross-linked to the substrate resulting in a stable ultrathin coating decorated with Y-shaped initiators. Weak PE A/B mixed brushes based on poly(methacrylic acid)/poly(2-vinylpyridine) (PMAA/P2VP) with a high grafting density of ∼1 chain/nm^2 are grown by surface-initiated ATRP and NMP, respectively. Detailed morphological characterization of the PMAA/P2VP brushes in response to pH changes reveals a nanoporous morphology under conditions that maximize complex coacervate formation between oppositely charged brushes. The charge ratio between the A and B brushes is varied via the composition of the brushes to further study the morphology evolution. The effect of intimate contact between the A and B brushes on the morphology is probed by comparing with a mixed A/B PE system with random fluctuations in grafting composition. A quantitative and qualitative study of the pore evolution with pH as well as charge composition is presented using a combination of atomic force microscopy, water contact angle measurement, and image analysis using Gwyddion software. These studies demonstrate that the porous morphology is enhanced and most uniform when the brushes are grown from the Y-inimer, indicating that a 1:1 grafting ratio and intimate contact between A and B brushes are essential.

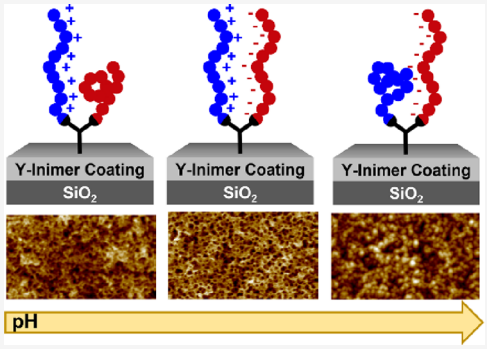

■ INTRODUCTION

Polyelectrolyte complex coacervates (PECCs) are formed by the interaction between two oppositely charged polymers in solution, which can undergo associative phase separation into a highly dilute solution phase and a condensed polymer-rich phase.[1−3] The complexation behavior of PECCs and the tunability in charges/charge densities have been explored for an array of potential applications ranging from encapsulation of proteins for drug and gene delivery,[4,5] assembly of conjugated polyelectrolyte donor−acceptor pairs in close proximity for optoelectronics or energy harvesting,[6,7] and underwater adhesives where the water-immiscible dense PECC phase can adhere to wet surfaces.[8,9] Hence, a number of theoretical and experimental studies have been directed at understanding their design principles and the resulting properties. The properties and formation of PECCs in bulk are primarily determined by both the electrostatic forces and the Flory−Huggins interaction parameter.[5] When the charge fraction is low, the Flory−Huggins interaction parameter or polymer backbone repulsion dominates and the polymers will separate into two phases, one of each polymer. Attractive electrostatic interactions dominate at a high charge fraction, and the polyelectrolytes form a complex, resulting in a new phase comprising both types of macromolecules.[10]

Although polyelectrolyte complexation has been studied for the past century, thin films of PECCs have been explored only in the past two decades.[11] Research in this area has primarily focused on the layer-by-layer (LBL) assembly of oppositely charged polyelectrolytes.[12,13] The phase behavior of PECCs in LBL assembly has yielded unique microporous polymer films that are being explored for applications in membrane separation and purification where specific pore sizes are needed to selectively exclude molecules of a certain size, supports for sensors and catalysts where nanoparticles can be incorporated into a pore structure of corresponding size,

Received: February 15, 2024
Revised: April 29, 2024
Accepted: April 30, 2024

scaffolds for tissue engineering where porosity can be tuned to target a high surface area for cell adhesion, and low-dielectric-constant materials where higher porosity allows a tunable decrease in the dielectric constant, among others.[14−17] LBL films often require a step-by-step fabrication process, and the stability of the films is often dictated by both the ionic strength and the pH. Cross-linking can be utilized to avoid delamination of PECCs with pH changes.[15] In comparison to the LBL method, PECC thin films can also be made by anchoring two oppositely charged polymers from one end to a substrate to create polyelectrolyte mixed brushes. In general, mixed A/B polymer brushes have primarily drawn interest in two main areas: the design of the nanoscale morphology[18−21] and the fabrication of responsive surfaces.[22−25] The interaction of A and B chains with each other and with the environment determines both the surface morphology and properties.[21,26−28] For example, when A and B are dissimilar, the immobility of the grafting points leads to microphase separation into a nanoscale morphology, while depending on the environment, A or B can also be preferentially exposed to the topmost surface, leading to switchable surface properties.[12,13,20] Mixed A/B PE brushes of opposite charges uniquely combine charge-switchable surface properties and the nanoscale morphology into one system.

Studies so far on PE brushes have mostly been limited to simulations[29−33] or homopolymers and copolymers.[34−38] Only one simulation study to date has explored the formation of lateral aggregates via microphase separation in mixed PE brushes. This study explored a relatively low grafting density regime and predicted the formation of lateral aggregates in a ripple structure when both polyelectrolytes were highly charged.[39] These predictions are not directly translatable to our studies where the grafting density is very high. Experimental studies are sparse and limited to low brush grafting density (<0.15 nm^{-2}).[40−42] The morphology of high grafting density mixed PE brushes with opposite charges remains unexplored. Compared to LBL films, the opposite charges in mixed PE brushes are positioned laterally across the surface instead of in a vertically layered arrangement, potentially leading to intimate lateral mixing of charges and smaller feature sizes. Experimental studies on mixed PE brushes with a long-range order and high grafting density are challenging mainly due to a lack of synthetic methods that are easy to implement in a scalable manner. To achieve high grafting density, grafting-from methods must be used. Most commonly, self-assembled monolayers (SAMs) have been used to grow homopolymer and mixed brushes by grafting-from methods.[43] To overcome some of the limitations of SAMs, such as limited stability to various reagents, substrate-dependent anchoring chemistry, degrafting of swollen brushes, and nonhomogeneous distribution of initiators,[43,44] and to achieve high grafting density A/B mixed brushes, we have developed ultrathin, cross-linkable inimer-containing coatings for brush growth using controlled radical polymerization methods.[18,45−47] These coatings contain either two types of inimers that can orthogonally grow A and B brushes, respectively, or a Y-shaped inimer that bears two distinct initiators attached at a single junction point for high grafting density mixed A/B brush growth by sequential surface-initiated atom transfer radical polymerization (SI-ATRP) and nitroxide-mediated polymerization (SI-NMP).[48,49] The Y-inimer coating is especially useful for the synthesis of mixed PE brushes as it ensures intimate contact between oppositely charged brushes and an equal grafting ratio.

In this article, we present the synthesis of highly dense mixed A/B brushes made of oppositely charged weak PEs and study their switchable surface morphology. We selected a widely studied model PE system, namely, poly(methacrylic acid)/poly(2-vinylpyridine) (PMAA/P2VP) brushes, as an example of oppositely charged weak polyelectrolytes to demonstrate the viability and versatility of the Y-inimer chemistry. The PMAA/P2VP brushes grown by SI-ATRP and SI-NM P, respectively, via a grafting-from approach from the Y-inimer coating ensures a1:1 stoichiometric grafting ratio of the two brushes. The growth of each of these brushes is well-controlled with a high grafting density of ∼1 chain/nm^2. Studies on the properties and morphology of the mixed PE brushes at varying pH values revealed a nanoporous morphology that is most pronounced at pH 6 and disappears at low and high pH extremes. We present a detailed analysis of the pore characteristics along with surface wettability changes at different pH conditions. The effect of the charge ratio of the A/B brushes on the morphology is studied by synthesizing poly(MAA-*co*-methyl methacrylate (MMA)) copolymer A brushes with varying compositions while keeping the B brush composition fixed. Mixed brushes with A and B chains randomly distributed across the substrate were created from a coating that has random fluctuations in the grafting composition of the two initiators, and the resulting morphology was compared to the Y-inimer case. Our results indicated that maximizing charge complex formation through a 1:1 grafting ratio of the brushes along with the intimate contact between A and B enabled by the Y-inimer design is necessary to achieve the most uniform, densely porous morphology. The versatility of this chemistry, access to high grafting density mixed PE A/B brushes, charge tunability, and the stability of the brushes can be widely applied to design robust polymer coatings with tunable and responsive nanopores.

■ EXPERIMENTAL METHODS

Materials. All solvents and reagents were purchased from Sigma-Aldrich Chemical Co. (Milwaukee, WI) and used without further purification unless otherwise specified. Glycidyl methacrylate (GMA) was stirred over calcium hydride and then distilled under vacuum and stored under Ar gas in the fridge. Ethyl α-bromoisobutyrate (EBiB) was distilled from CaH_2 and stored at 2 °C. 2-Vinylpyridine (2VP) was stirred over calcium hydride and then distilled under vacuum at 40 °C and stored under Ar gas in the fridge. Styrene (S), *tert*-butyl methacrylate (tBMA), and methyl methacrylate (MMA) were filtered through basic alumina before use. 2,2′-Azobis(2-methylpropionitrile) (AIBN) was recrystallized from methanol and dried under vacuum. The Y-inimer was synthesized through a multicomponent reaction using a formamide methacrylate monomer according to our previous work (Figure S1).[49] An ATRP inimer and an NMP inimer were synthesized according to our previous reports.[45,46] A free NMP initiator was synthesized from a reported procedure.[59] Si(100) wafers were test-grade wafers purchased from UniversityWafer, Inc.

Characterization. Size exclusion chromatography (SEC) of the Y-inimer copolymer, mixed inimer copolymer, and PtBMA was performed using a Viscotek 2210 system equipped with three Waters columns (HR4, HR4E, and HR3). THF was used as the eluent with a flow rate of 1 mL/min at 30 °C. The calibration curve for analysis consisted of nine narrow dispersity PS standards with M_n from 1 to 400 kg/mol. SEC of P2VP was performed using a Shimadzu LC-40D pump with two inline Agilent PLgel columns, a Wyatt Technology DAWN Heleos II light scattering detector, and a Wyatt Technology Optilab T-rEX refractive index detector. HPLC-grade DMF with 0.05 M LiBr was used as the mobile phase with a flow rate of 1 mL/min. The absolute weight-average molecular weight of P2VP was

https://doi.org/10.1021/acs.langmuir.4c00556
Langmuir XXXX, XXX, XXX−XXX

determined using the dn/dc value of 0.1444 mL/g in DMF. ^{1}H NMR spectra were recorded in $CDCl_3$ with a TMS internal standard using a Bruker Avance 400 spectrometer. Film thickness was measured by ellipsometry using a Rudolph Research Auto EL at three wavelengths (632.8, 546.1, and 405 nm). Scanning electron microscopy (SEM) images were acquired using a Zeiss Gemini 450 FESEM or a Zeiss Gemini 300 FESEM at a 1 kV accelerating voltage. Atomic force microscopy (AFM) images were acquired using a Bruker Dimension Icon with ScanAsyst probe tips in the tapping mode. Contact angle measurements were performed using a DataPhysics OCA 15 plus contact angle measuring device. pH values of the aqueous baths were measured using a Fisherbrand accumet AE150 benchtop pH meter.

Y-Inimer Coating Copolymerization. A Y-inimer (0.1262 g, 0.21 mmol), glycidyl methacrylate (GMA) (17.3 mg, 16.2 μL, 0.11 mmol), azobis(isobutyronitrile) (AIBN) (1.4 mg, 0.01 mmol), and anisole (0.5 mL) were added to a Schlenk flask. The solution was then purged with Ar for 30 min and then heated up to 70 °C for 18 h. The copolymer was purified by precipitating in hexane 5 times to yield a red to yellow solid. The composition of the copolymer from ^{1}H NMR quantification was 50:50 Y-inimer:GMA (Figures S2 and S3).

Mixed Inimer Coating Copolymerization. An NMP inimer (0.574 g, 2.34 mmol), an ATRP inimer (0.307 g, 1.27 mmol), GMA (0.114 g, 0.94 mmol), styrene (0.238 g, 2.67 mmol), AIBN, 4-cyano-4-[(dodecylsulfanylthiocarbonyl)sulfanyl]pentanoic acid (0.0094 g, 0.067 mmol), CDSPA (0.0046 g, 0.0134 mmol), and anisole (2 mL) were added to a Schlenk flask. The solution was then purged with Ar for 30 min and heated at 70 °C for 18 h. The copolymer was purified by precipitating into methanol 3 times to yield a white powder. The composition of the copolymer from ^{1}H NMR quantification (Figure S4) was [ATRP]:[NMP]:[styrene]:[GMA] = 23:23:38:16.

Substrate Preparation and Thin-Film Formation. Si(100) substrates were cleaned with piranha acid (H_2SO_4:H_2O_2 = 3:1, highly explosive when in contact with organics). A Y-inimer coating copolymer solution in toluene (0.15 wt %) or a mixed inimer copolymer solution in toluene (0.10 wt %) was spin-coated onto the cleaned wafers and annealed under vacuum at 120 °C for 30 min to cross-link the film. Chains that were not cross-linked were removed by soaking the coatings in toluene for 30 min and rinsing with a copious amount of toluene. The coatings were dried under nitrogen and stored in the fridge.

Poly(*tert*-butyl methacrylate) (PtBMA) Brush Growth. PtBMA brushes were grown using activators regenerated by electron transfer (ARGET) ATRP. $CuBr_2$ (0.0011 g, 0.046 mmol) and tris[2-(dimethylamino)ethyl]amine (Me_6TREN) (0.012 mL, 0.46 mmol) were mixed in anisole (3 mL) in a 10 mL Schlenk flask and sonicated until a light green/yellow uniform mixture was obtained. tBMA (3 mL, 18.4 mmol) and EBiB (0.0068 mL, 0.46 mmol) were then added, and the mixture was degassed by argon bubbling for 30 min. After 30 min, tin(II) 2-ethylhexanoate ($Sn(EtH)_2$) (0.015 mL, 0.46 mmol) was added along with a Si wafer coated with either Y-inimer or mixed inimer coating, and the mixture was further degassed for 5 min until it became transparent. The reaction was placed in an oil bath at 60 °C for the desired amount of time. The substrate with the PtBMA brushes was soaked in THF overnight and then sonicated for 10 min to remove unattached chains. The polymer from solution was precipitated into a 50/50 v/v solution of water and methanol. The thickness of the brush was measured by ellipsometry.

Substitution of the PtBMA Chain End. Azobis(isobutyronitrile) (AIBN) (0.025 g, 0.15 mmol), tributyltin hydride (0.25 mL, 0.91 mmol), and the substrate were added to a Schlenk flask with anisole (10 mL) and degassed by Ar bubbling for 30 min. The system was heated to 60 °C for 3 h. Wafers were removed and rinsed copiously with THF and dried.

Poly(*tert*-butyl methacrylate-*co*-methyl methacrylate) (Poly(tBMA-*co*-MMA)) Brush Growth. In the charge ratio variation experiments, poly(tBMA-*co*-MMA) was grown as the A brush. PMMA is not a polyelectrolyte, so it was used to decrease the amount of negative charge in the A brush. Poly(tBMA-*co*-MMA) was grown with ARGET ATRP following the same procedure above, but MMA was included as a comonomer with tBMA. The feed ratio of tBMA to MMA was adjusted to obtain poly(tBMA$_{20}$-*co*-MMA$_{80}$), poly(tBMA$_{50}$-*co*-MMA$_{50}$), and poly(tBMA$_{80}$-*co*-PMMA$_{20}$) brushes. Copolymer compositions of the brushes were confirmed by NMR of the polymer formed in solution. After growth of P2VP as the B brush, the PtBMA was deprotected to yield PMAA as described below.

Poly(2-vinylpyridine) (P2VP) Brush Growth. 2VP (3 mL, 27.8 mmol), the free initiator 1-phenyl-1-(2,2,6,6-tetramethyl-1-piperidinyloxy)ethane (0.015 g, 0.056 mmol), and anisole (3 mL) were mixed in a Schlenk flask with a substrate containing NMP initiators. The flask was degassed by argon bubbling for 30 min and then immersed in a 135 °C oil bath for the desired amount of time. The flask was removed from the oil bath and cooled under running water. The substrates were removed from the flask and washed with THF. After washing, the substrates were soaked in THF overnight and sonicated for 10 min and dried under nitrogen. The polymer from solution was precipitated into hexane. The thickness of the brush was measured using ellipsometry.

Substitution of the P2VP Chain End. The substrates with mixed brushes were placed in a solution of 1-dodecanethiol (0.17 mL, 0.72 mmol) and anisole (8 mL) in a 10 mL Schlenk flask. The solution was degassed by purging with argon gas for 30 min. The flask was heated in an oil bath at 135 °C for 1 h. After cooling to room temperature, the wafers were removed and rinsed thoroughly with THF and dried under nitrogen.

Grafting Density Calculation. Grafting densities of the brushes were calculated based on the thickness of the brush (h) and the molecular weight of the polymer formed in solution ($\bar{M}_n$)using the following equation:

$$\sigma = \frac{h\rho N_A}{\bar{M}_n}$$

where N_A is Avogadro's number and ρ = 1.02 g/cm^2 for PtBMA and ρ = 1.15 g/cm^2 for P2VP. The height of the B brush was calculated by subtracting the height of the A brush from the total mixed brush height according to our previous method.[18] Previous work has shown that the molecular weight of the polymer grown in solution during SI-ATRP is a relatively good estimate of the molecular weight of the brush.[18,46,50,51] However, for SI-NMP, we have shown that brushes cleaved from the surface have ~1.56 times higher molecular weight than the polymers in solution.[45] Based on these previous studies, a correction factor of 1.56 was used to calculate the adjusted molecular weight of the P2VP brushes on the surface.

Deprotection of the *tert*-Butyl Groups on the PtBMA Brushes. After growth of both brush components and chain end substitution, the PtBMA/P2VP brushes were immersed in a solution of 10% v/v trifluoroacetic acid in DCM overnight. Wafers were removed and rinsed thoroughly and soaked in DI water.

pH Variation Experiments. Aqueous baths at different pH values were prepared using either hydrochloric acid or sodium hydroxide in DI water (DI water for pH 6, 10 and 0.1 mM HCl for pH 2 and pH 4, respectively, and 0.001, 0.1, and 10 mM NaOH for pH 8, pH 10, and pH 12, respectively). Wafers containing polymer brushes were soaked in the desired solution for at least 3 h and rapidly dried before analysis.

Pore Analysis. Pores were analyzed using the Gwyddion software package. The pores in each of the images were distinguished and marked using the watershed algorithm. In the watershed algorithm, virtual water droplets are placed on the test surface, and their free spreading is numerically simulated. The virtual water drops follow the steepest descent path to minimize potential energy, stopping when they reach a local minimum. Drops partially fill the local minimum with their volume resulting in "lakes" that are interpreted as pores. The process was controlled by both the drop size and the number of steps to achieve the best marking of pores across the sample. Based on the watershed process, pores were quantified based on the equivalent disc radius, projected area, pore volume, and total pore area.

https://doi.org/10.1021/acs.langmuir.4c00556
Langmuir XXXX, XXX, XXX−XXX

Scheme 1. Schematic Overview of the Chemical Structure of the Y-Inimer Coating and Growth of Mixed A/B PE Brushes with Opposite Charges (PMAA and P2VP) to Form a Polymer Brush Complex Coacervate

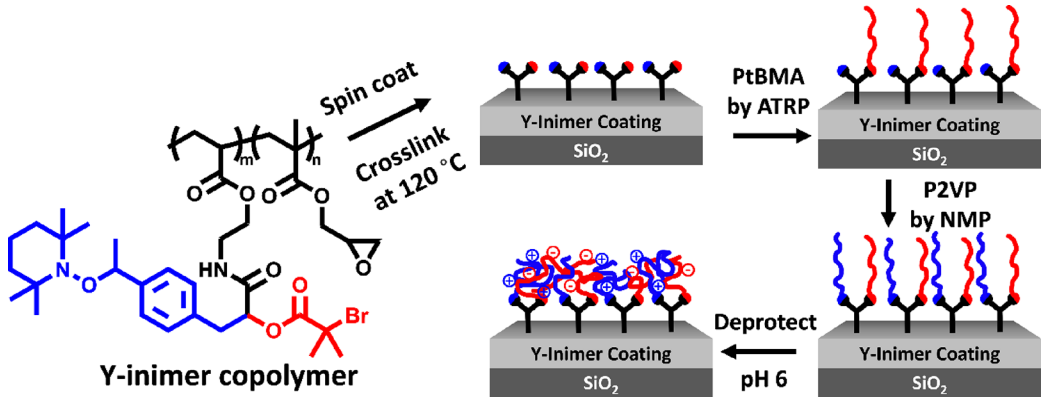

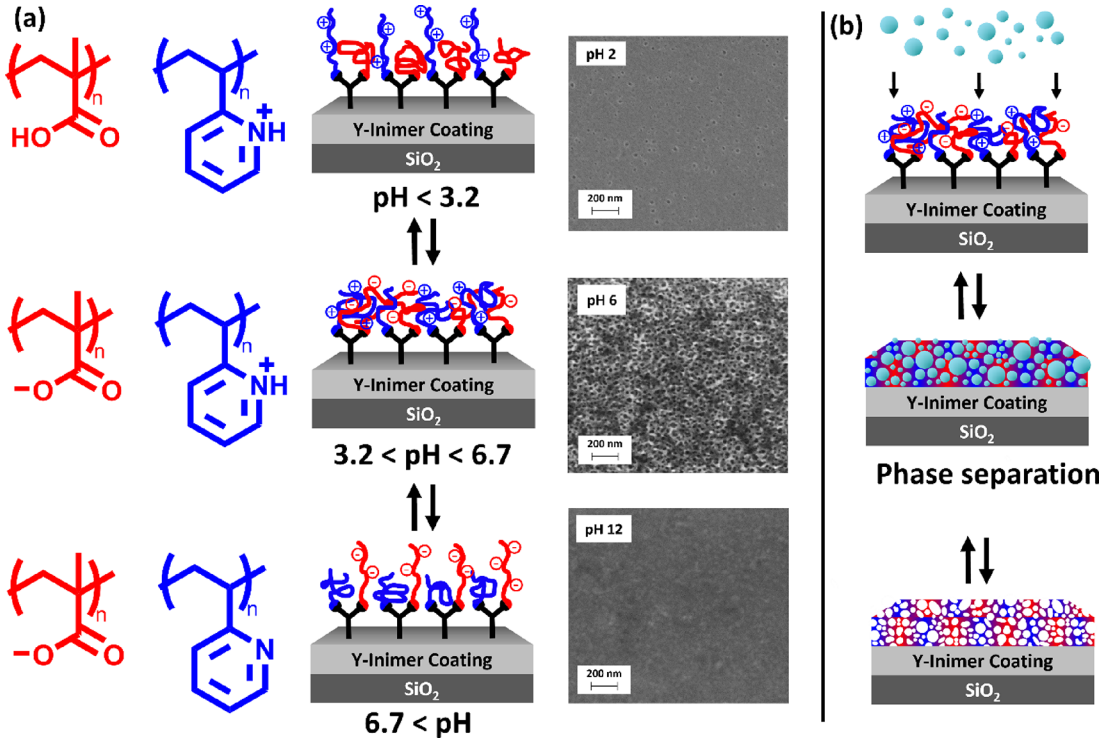

Figure 1. (a) Schematic overview of surface charge and brush conformation for the PMAA/P2VP mixed brush depending on the pH along with corresponding SEM images at pH 2, 6, and 12. pH was adjusted by adding HCl or NaOH to the aqueous bath at the appropriate concentration (DI water for pH 6, 10 mM HCl for pH 2, and 10 mM NaOH for pH 12). The grafting densities of the PMAA and P2VP brushes were 1.09 and 1.00, respectively (Table S1). SEM images show a switchable porous morphology. (b) Schematic showing the proposed mechanism for formation of pores at pH between 3.2 and 6.7. Mixed A/B PE brushes form complexes that undergo phase separation in aqueous conditions, and pores remain after rapid drying of the sample.

■ RESULTS AND DISCUSSION

Design and Synthesis. Mixed A/B PECC brushes were synthesized by a grafting-from method using a previously developed Y-shaped inimer-bearing coating with ATRP and NMP initiators.[49] Y-shaped initiators are unique because they contain two orthogonal initiators attached at a common junction point, which ensures a 1:1 grafting ratio and intimate contact of subsequently grown polymers across the entire substrate. The Y-inimer was synthesized using a previously developed one-pot multicomponent reaction to incorporate both initiators into one monomer unit (Figure S1). The Y-inimer was then copolymerized with glycidyl methacrylate (GMA) by free radical polymerization to form poly(Y-inimer-*r*-GMA) with a 1:1 ratio of the Y-inimer to GMA according to our previously developed method (Figures S2 and S3).[49] A poly(Y-inimer-*r*-GMA) solution in toluene was spin-coated onto silicon substrates, and the epoxide group in GMA was cross-linked by thermal annealing at 120 °C to form a stable coating with a 1:1 ratio of ATRP and NMP initiators that could withstand subsequent brush growth conditions (Scheme 1). Coatings with a thickness between 3 and 4 nm were targeted by spin coating a 0.15 wt % solution of the copolymer.

The intimate mixing between the A and B chains facilitated by the Y-architecture is especially attractive to explore polyelectrolyte complexation behavior between oppositely charged brushes. Mixed PMAA/P2VP brushes were synthe-

https://doi.org/10.1021/acs.langmuir.4c00556
Langmuir XXXX, XXX, XXX−XXX

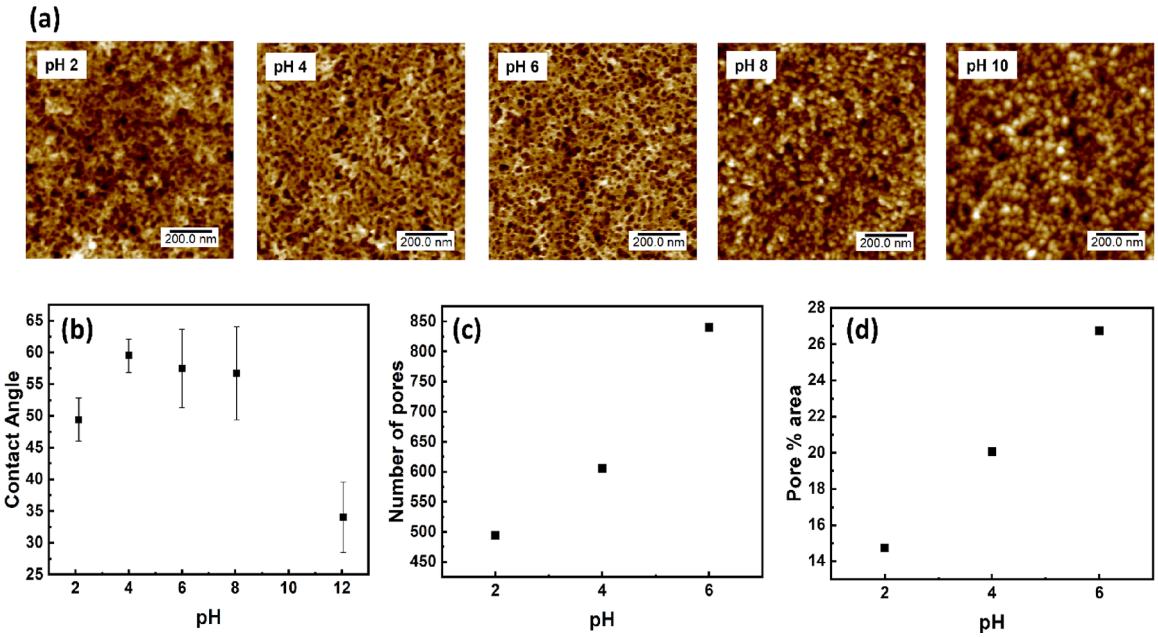

Figure 2. (a) AFM images of the PMAA/P2VP mixed brushes showing the morphology after exposure to aqueous baths ranging from pH 2 to 10. pH was adjusted by adding HCl or NaOH to the aqueous bath at the appropriate concentration (DI water for pH 6, 10 and 0.1 mM HCl for pH 2 and pH 4, respectively, and 0.001 and 0.1 mM NaOH for pH 8 and pH 10, respectively). (b) Water contact angle after exposure to different pH values. Water contact angles are the highest when the PECC forms at middle pH values and the lowest when the surface has a net positive or negative charge at the pH extremes. (c) Number of pores for samples exposed to pH 2, 4, and 6. (d) Pore % area for samples at pH 2, 4, and 6. There are the greatest number of pores and the highest pore % area at pH 6 when the complex coacervate forms.

sized as an example of weak polyelectrolytes with opposite charges (Scheme 1) from the Y-inimer coating. Poly(*tert*-butyl methacrylate) (PtBMA) brushes were first grown by SI-ATRP as protected analogues to PMAA brushes. To prevent interference with the growth of P2VP brushes by SI-NMP in the subsequent step, the bromine chain ends from the ATRP initiator were substituted with a proton. After the SI-NMP of P2VP, the nitroxide end groups were substituted with a proton.[52] In the final step, the PtBMA brushes were deprotected with trifluoroacetic acid (TFA) in dichloromethane (DCM) resulting in the targeted PMAA/P2VP mixed brush. The water contact angle decreased from 94 to 44.5°, upon deprotection of the *tert*-butyl group confirming the formation of a more hydrophilic PMAA (Figure S5).

Morphology Evolution with pH. Top-down SEM of the deprotected mixed brushes did not show a porous morphology before soaking in an aqueous bath (Figure S6). Both PMAA and P2VP are weak PEs; hence, the charge density is a function of the pH. Mixed PMAA/P2VP brushes were placed in aqueous solutions with varying pH and dried to study the surface properties and morphology of the brushes. At 3.2 < pH < 6.7, both polymers were charged and interacted to form a complex, which was evident from the evolution of a porous morphology as observed by SEM (Figure 1a). This porous morphology resulted from the formation of a complex coacervate and phase separation into a polymer-rich phase and a dilute solution phase. After drying and exclusion of water, pores remained in place of the dilute solution phase (Figure 1b). Simulations of low grafting density mixed polyelectrolyte brushes show laterally isolated aggregates due to complex coacervation.[39] Our system has a much higher grafting density than the system studied in simulation. At a high grafting density, the solvent is the minority species; hence, inverted solvent micelles (pores) are formed as the solvent minimizes surface contact with the coacervate phase. This is consistent with simulations by Pattanayek et al. showing hole formation in high density polymer brushes in poor solvents.[53] The porous morphology was indeed switchable with pH. At pH below 3.2, the protonated P2VP is positively charged, and the PMAA remains neutral; meanwhile, at pH above 6.7, deprotonated PMAA is negatively charged, and P2VP remains neutral. At the extreme pH values, the highly porous structure disappeared as the brushes no longer engaged in complex coacervation, and the morphology was instead controlled by incompatibility between the two brushes. Homopolymer brushes of PMAA and P2VP were studied as controls. SEM analysis of these homopolymer brushes subjected to the same conditions as the Y-shaped mixed brushes did not display any porous morphology, indicating that the complexation of the PEs was necessary for formation of nanopores (Figure S6).

Detailed AFM analysis at five different pH conditions is shown in Figure 2a along with corresponding water contact angles (Figure 2b). Brushes were exposed to aqueous baths at pH 2, 4, 6, 8, and 10 and rapidly dried for analysis. AFM in solution showed a similar porous morphology (Figure S7). Qualitatively, the brush had the most porous morphology after exposure to pH 6 conditions. This is consistent with the fact that at the middle pH values (between 3.2 and 6.7), both brushes are charged, and the PECC can form. Some pores were still present after exposure to pH 4 and pH 2, but as the pH decreased, the brush appeared less porous, and the pores that existed appeared less uniform in size and shape, especially at pH 2. After exposure to pH 8 and 10, the nanoporous morphology disappeared and was replaced by a nanoscale mixed brush morphology. These observations are consistent with the fact that at the pH extremes, only one of the brushes is charged, eliminating the associative interactions of PMAA and P2VP, and the morphology is dictated primarily by the

https://doi.org/10.1021/acs.langmuir.4c00556
Langmuir XXXX, XXX, XXX−XXX

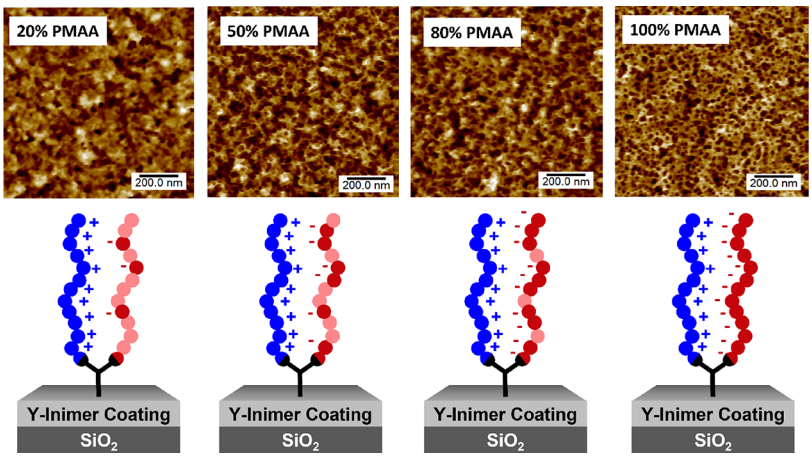

Figure 3. AFM images of mixed A/B polyelectrolyte brushes with varying charge ratios. As shown in the schematics below, the charge ratio was varied by growing a poly(MAA-*co*-MMA) copolymer as the A brush with 20, 50, 80, and 100% of PMAA units (PMAA shown in red, PMMA shown in pink, and P2VP shown in blue). Grafting densities for all brushes were between 0.75 and 1.2 chains/nm^2 (Table S2). The most uniform porous structure was observed in the 100% PMAA case where the charge ratio was equal (far right).

incompatibility between the two brushes. Similar to the studies on the P2VP-*b*-PAA polyampholyte system[54] where at high pH, the P2VP is not protonated and hydrophobic while PAA remains negatively charged and hydrophilic leading to micelle formation with PAA in the corona, it is likely that the morphology that we observe at the high pH of 10 (Figure 2) is also a micellar aggregate. The changes in surface charges were apparent in the contact angle measurements. At the low and high pH extremes (2 and 10), the surface is charged with either protonated P2VP or deprotonated PMAA, respectively, and thus, contact angles were relatively low (50 and 34°, respectively). In the midrange pH values, a maximum contact angle of 60° is reached due to complexation that results in charge neutralization making the surface more hydrophobic. Qualitatively, the SEM agrees with the AFM images (Figure S8). The cross-linked inimer coating was robust enough that there was minimal degrafting of swollen brushes after exposure to different pH conditions, with brushes retaining 90% of their original thickness after overnight soaking at the pH extremes.

Quantitative information about pores, such as the equivalent pore radius distribution, can be obtained through statistical analysis of SEM and TEM images.[55,56] In image analysis, it is often challenging to accurately and systematically mark pores, and the information is typically derived only from the top surface of the sample. AFM is one of the best existing methods to analyze nanoscale pore structures because the imaging is in three dimensions. This means that in addition to 2D pore characteristics such as the diameter and area, 3D characteristics such as the pore volume can also be analyzed.[57] Furthermore, several types of software have been developed for statistical analysis of features in AFM images. Gwyddion is one such open-source AFM image processing software that has been widely used to mark and quantify pores using grayscale images to represent the height of the sample surface.[57−59] Therefore, the pore characteristics of the mixed PE brushes synthesized were analyzed quantitatively using the watershed algorithm for AFM grain analysis in Gwyddion software. The watershed algorithm marks and classifies pores based on local minima across the sample surface (more details in the experimental section). Although the watershed algorithm overcomes some of the issues of marking pores in more complicated structures when there is a lot of local height variation, no pore marking algorithm is perfect, and these methods tend to work less well over larger sample areas. The pores in the AFM images from the pH 2, 4, and 6 conditions in Figure 2 were first marked using the watershed algorithm (Figure S9), and then, the equivalent disc radius and pore volume were extracted along with the total number of pores and total pore area (Figure 2c,d and Table S3). Based on this analysis, the number of pores per μm^2 decreased by 41% as the pH decreased from pH 6 to pH 2. Similarly, the pore % area decreased from 27 to only 15% of the total area (Figure 2c,d). The median pore volume also clearly decreased from 1180 μm^3 at pH 6 to 777 μm^3 at pH 4 to 293 μm^3 at pH 2 (Table S3). These results show that PECC formation is necessary to maximize the nanoporous brush morphology.

Morphology Modulation by the Charge Ratio. The effect of the charge ratio between the A/B brushes at pH 6 was investigated by synthesizing a series of mixed PE brushes with poly(MAA-*co*-MMA) copolymers with varying mole % of PMAA (20, 50, 80, and 100%) as the A brush, while the B brush was fixed as the P2VP homopolymer as before. As PMMA is not a polyelectrolyte, increasing the PMMA mole % resulted in lower charge density in the A brush and hence an increasing charge imbalance between the A and B brushes at pH 6. By controlling the feed ratio of the tBMA:MMA monomers in the SI-ATRP of the A brush, the resulting brush composition was predictably controlled. NMR analysis of the solution poly(MAA-*co*-MMA) was used to estimate the copolymer composition (Figure S10). The resulting surface morphology was studied by AFM (Figure 3). Qualitatively, the poly(MAA$_{20}$-*co*-MMA$_{80}$)/P2VP brushes showed the fewest pores, compared to the poly(MAA$_{50}$-*co*-MMA$_{50}$)/P2VP and poly(MAA$_{80}$-*co*-MMA$_{20}$)/P2VP brushes. Irrespective of the composition, all three brushes showed a large variability in pore sizes and spacing. In comparison, the PMAA/P2VP brushes showed the most pores with a relatively regular pore spacing and size. This indicated that equal mixing of the opposite charges is essential to maximize the porous structure in the polymer brushes.

Quantitative pore analysis for the samples with varied charge ratios was done with the watershed algorithm using Gwyddion software (Figure S11) as described above, and the pore characteristics were summarized by the median and range disc

https://doi.org/10.1021/acs.langmuir.4c00556
Langmuir XXXX, XXX, XXX−XXX

(a)

PMAA amount (%)	Disc radius (nm)		Pore volume (nm³)		Total Pores
	Median	Range	Median	Range	
100	8.50	26.5	1180	25,300	840
80	8.81	34.9	754	53,100	590
50	6.91	33.0	455	41,700	666
20	7.46	20.8	219	7250	533

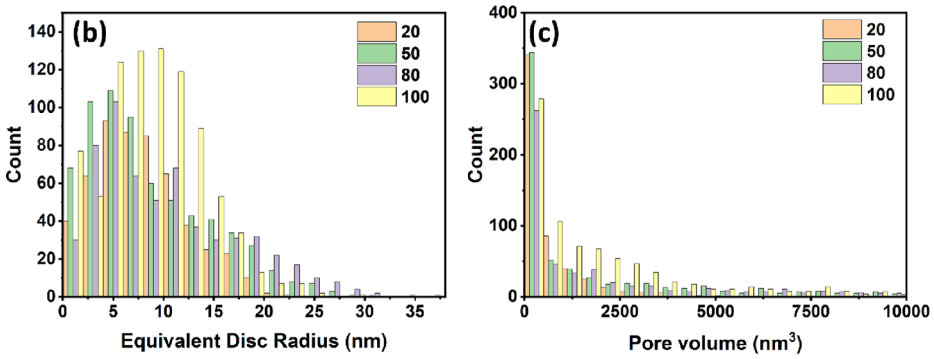

Figure 4. Pore characteristics analyzed using Gwyddion software. (a) Median and range for the pore disc radius and pore volume along with the total number of pores for samples with varying charge ratios between A and B brushes. (b,c) Histograms are shown for the disc radius and pore volume.

Scheme 2. Schematic Overview for the Chemical Structure of the Mixed Inimer Coating, Thermal Cross-Linking, and Growth of Mixed A/B PE Brushes with Opposite Charges (PMAA and P2VP) to Form a Polymer Brush Complex Coacervate

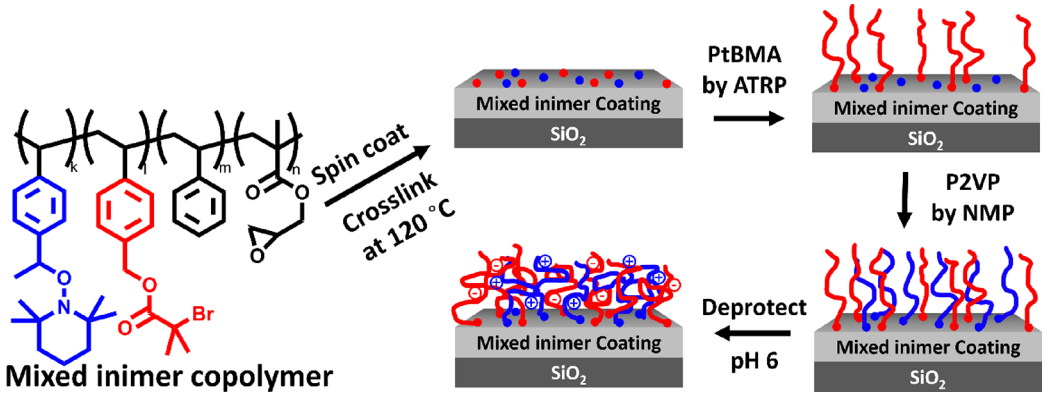

radius and volume, along with the total number of pores (Figure 4a). The distribution of pore sizes in each brush was further visualized and compared through histograms of the pore disc radius and pore volume (Figure 4b,c). As the mole % of PMAA in the A brush decreased from 100 to 20%, the number of pores decreased by 60%. This indicated that an increasing mismatch in the ratio of negative and positive charges decreased the pore formation. Both the poly(MAA_{50}-*co*-MMA_{50})/P2VP and poly(MAA_{80}-*co*-MMA_{20})/P2VP brushes had more pores than the poly(MAA_{20}-*co*-MMA_{80})/P2VP brush. Based on the range and distribution plots for the disc radius and pore volume, the pores in the (MAA_{50}-*co*-MMA_{50})/P2VP and (MAA_{80}-*co*-MMA_{20})/P2VP brushes were less uniform than in the PMAA/P2VP brushes. For example, the range for the disc radius in the PMAA/P2VP brush was only 26.5 nm compared to 33.0 and 34.9 nm in the (MAA_{50}-*co*-MMA_{50})/P2VP and (MAA_{80}-*co*-MMA_{20})/P2VP brushes, respectively. A similar trend was observed for the pore volume. A second set of images at a different spot on the sample surface was also analyzed, and the trends were found to be similar, indicating consistency across the sample surface (Table S4). Together, these results confirmed that similar amounts of positive and negative charges are needed to obtain a mixed brush with the most dense and uniform pore structure.

Morphology Changes with Variations in Local Initiator Distribution from a Mixed Inimer Coating. Simulations have shown that inhomogeneous grafting compositions in mixed polymer brushes can influence the resulting morphology.[60] To study if the porous morphology of the PMAA/P2VP mixed PE brushes is influenced by the proximity of A and B chains with an equal grafting ratio, we synthesized PMAA/P2VP mixed PE brushes from an inimer coating with locally random fluctuations in the grafting composition of the two initiators (mixed inimer coating). In this mixed inimer coating, the NMP and ATRP initiator-bearing monomers (inimers) were copolymerized with GMA and styrene and cross-linked onto the substrate, as compared to the Y-inimer coating where the ATRP and NMP initiators

https://doi.org/10.1021/acs.langmuir.4c00556
Langmuir XXXX, XXX, XXX−XXX

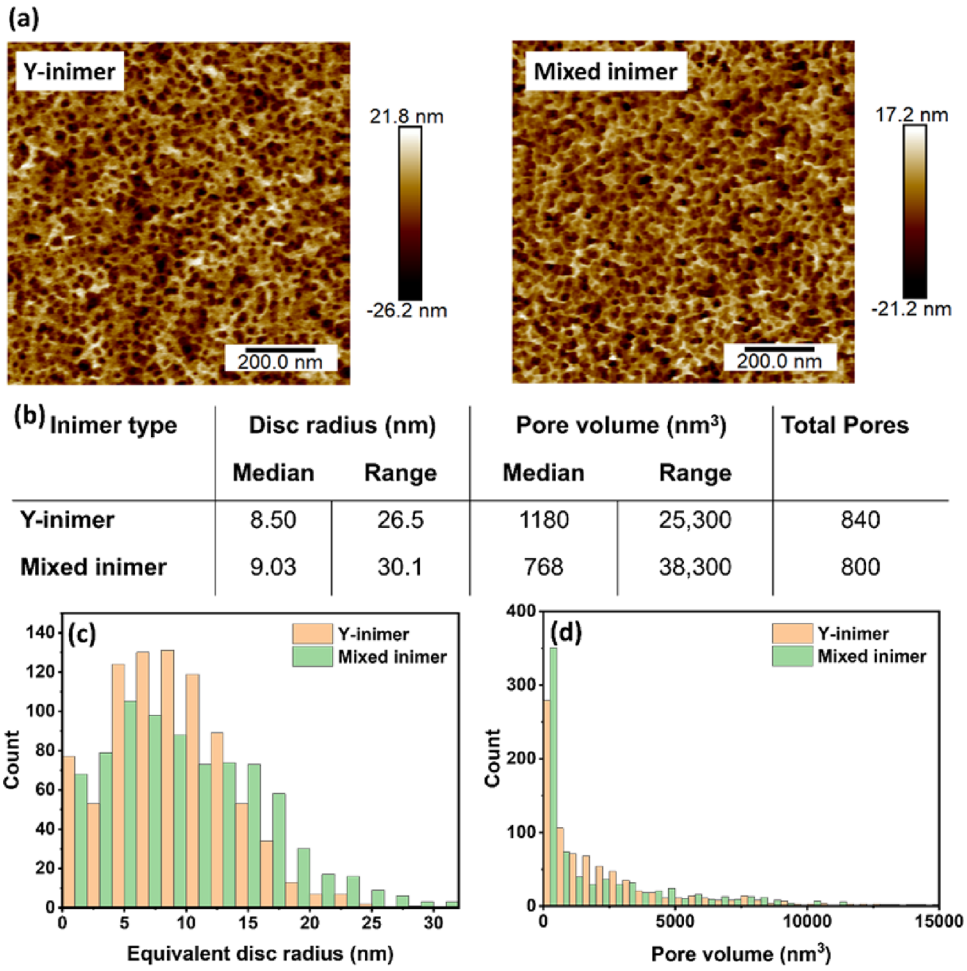

Inimer type	Disc radius (nm)		Pore volume (nm³)		Total Pores
	Median	Range	Median	Range	
Y-inimer	8.50	26.5	1180	25,300	840
Mixed inimer	9.03	30.1	768	38,300	800

Figure 5. Comparison of the porous morphology in mixed PMAA/P2VP brushes grown from a Y-inimer coating and a mixed inimer coating. Grafting densities of the Y-inimer brushes were 1.09 and 1.00 chains/nm^2 for the PMAA and P2VP, respectively, while grafting densities of the mixed inimer brushes were 0.71 and 0.58 chains/nm^2 (Table S1). (a) AFM images for the two samples both showed a highly porous structure. (b) Analysis of the pore characteristics using Gwyddion software showed that the pores are more uniform in the Y-inimer sample, which can be visualized in the (c) histograms for the equivalent disc radius and pore volume.

are attached to a common Y-junction in a single monomer unit (Scheme 2).

We synthesized the previously developed mixed inimer coating with a copolymer composition that contained an overall equal mole ratio of ATRP and NMP initiators (ATRP:NMP:styrene:GMA ratio of 23:23:38:16).[18] Even though globally, on the surface, the distribution of the two initiators is in a 1:1 ratio, this does not necessarily translate locally into a 1:1 grafting composition. After thermally cross-linking the mixed inimer copolymer to the substrate, brushes were grown using the same sequential process as with the Y-inimer, and the pore structure was studied by AFM (Figure 5).

Qualitatively, the AFM images were relatively similar, and both samples were highly porous (Figure 5a). Based on the analysis of the pores using the Gwyddion watershed algorithm, the samples had an approximately equal number of pores (840 and 800 for the Y-inimer and mixed inimer, respectively); however, the pores in the Y-inimer sample were smaller and more uniform and formed a denser network (Figure 5b,c). The median disc radius and pore volume in the Y-inimer sample were smaller than in the mixed inimer sample (8.50 nm compared to 9.03 nm), indicating smaller pores in the Y-inimer sample. However, the median pore volume was higher in the Y-inimer sample (1180 nm^3 compared to 768 nm^3), indicating that the 3D pore network was denser and more interconnected in the Y-inimer sample. The range for the disc radius and pore volume was also smaller for the Y-inimer, indicating a narrower distribution of pore sizes for the Y-inimer sample, which can be visualized in the histograms for the equivalent disc radius and pore volume (Figure 5c). Typically, in mixed brushes, there is a relatively thick crossover zone of the two brushes near the substrate. Simulation results show that the mixed region occupies about 10−15% of the total thickness, and it is not affected by the grafting density but increases with decreasing segregation strength between A and B brushes.[18] This crossover region is eliminated when the Y-architecture for the mixed polyelectrolyte system is used. Hence, the Y-inimer coating has a unique ability to ensure intimate mixing and an equal grafting ratio across the surface for the oppositely charged polyelectrolytes and thus leads to the most uniformly porous brush structure.

■ CONCLUSIONS

In conclusion, we have grown high density mixed A/B polymer brushes made of weak polyelectrolytes, PMAA and P2VP, of opposite charges from a Y-shaped inimer coating. The unique structure of the Y-inimer, where orthogonal initiators for

https://doi.org/10.1021/acs.langmuir.4c00556
Langmuir XXXX, XXX, XXX−XXX

growth of the A and B brushes are attached at a common junction point, ensured an equal grafting ratio and intimate mixing of the oppositely charged PMAA and P2VP brushes, leading to formation of a complex coacervate brush and a porous morphology. Due to the charge switching at different pH, the porous morphology could be switched on and off by exposing the brush to aqueous conditions with different pH. By growing poly(MAA-*co*-MMA) for the A brush, the ratio of negative to positive charges could be systematically controlled. Samples with a greater discrepancy in the charge ratio showed fewer and less uniform pores in AFM, indicating that a similar charge ratio is necessary to achieve the porous morphology. Finally, PMAA/P2VP brushes grown from a mixed inimer coating, where the local ratio of initiators can vary and poses a crossover region near the substrate, showed a less uniform pore structure. These studies reveal that the intimate mixing of the two brushes in a 1:1 grafting ratio enabled by the Y-inimer leads to the most uniformly porous brush structure. These studies also confirm that local random fluctuations in the grafting ratio of the two brushes even if the overall grafting ratio is 1:1 can still affect the pore size distribution. Polyelectrolyte complex coacervate formation is one example where the 1:1 grating ratio of A and B enabled by the Y-inimer is critical. Our Y-inimer has broader utility in other systems where a 1:1 grafting ratio and intimate mixing of two brushes are desirable, such as donor/acceptor pairs and phase separation of high-χ mixed brushes.

■ ASSOCIATED CONTENT

Supporting Information

The Supporting Information is available free of charge at https://pubs.acs.org/doi/10.1021/acs.langmuir.4c00556.

Additional characterization information, including ^{1}H NMR spectra, GPC, brush molecular weight, thickness, and grafting density values, contact angle, SEM, and details of pore analysis using Gwyddion (PDF)

■ AUTHOR INFORMATION

Corresponding Author

Padma Gopalan − *Department of Chemistry and Department of Materials Science and Engineering, University of Wisconsin-Madison, Madison, Wisconsin 53706, United States;* orcid.org/0000-0002-1955-640X; Email: pgopalan@wisc.edu

Authors

Julia D. Smith − *Department of Chemistry, University of Wisconsin-Madison, Madison, Wisconsin 53706, United States;* orcid.org/0009-0008-9715-9101

Ri Chen − *Department of Materials Science and Engineering, University of Wisconsin-Madison, Madison, Wisconsin 53706, United States*

Nicolas Noriega Osores − *Department of Materials Science and Engineering, University of Wisconsin-Madison, Madison, Wisconsin 53706, United States*

Complete contact information is available at: https://pubs.acs.org/10.1021/acs.langmuir.4c00556

Notes

The authors declare no competing financial interest.

■ ACKNOWLEDGMENTS

J.D.S., R.C., and P.G. acknowledge support for this work by the National Science Foundation: DMR-2003891 and DMR-1507409. P.G. and R.C. acknowledge partial support for this research by the University of Wisconsin-Madison, Office of the Vice Chancellor for Research and Graduate Education with funding from the Wisconsin Alumni Research Foundation. We gratefully acknowledge support from the staff and use of the facilities and instrumentation at the UW-Madison Wisconsin Centers for Nanoscale Technology (wcnt.wisc.edu) partially supported by the NSF through the University of Wisconsin Materials Research Science and Engineering Center (DMR-1720415). We are especially grateful for the support from Dr. Julie Morasch and Dr. Nick Bulloss during AFM imaging. The Bruker Avance 400 NMR spectrometer was supported by NSF grant CHE-1048642. P.G. and J.D.S. also acknowledge discussions with Prof. David Lynn on potential applications of these brushes and with Dr. Sean Michael Foradori on the AFM analysis.

■ REFERENCES

(1) Rumyantsev, A. M.; Jackson, N. E.; de Pablo, J. J. Polyelectrolyte Complex Coacervates: Recent Developments and New Frontiers. *Annu. Rev. Condens. Matter Phys.* **2021**, *12*, 155−176.

(2) Zhou, L.; Shi, H.; Li, Z.; He, C. Recent Advances in Complex Coacervation Design from Macromolecular Assemblies and Emerging Applications. *Macromol. Rapid Commun.* **2020**, *41* (21), 2000149.

(3) Neitzel, A. E.; Fang, Y. N.; Yu, B.; Rumyantsev, A. M.; de Pablo, J. J.; Tirrell, M. V. Polyelectrolyte Complex Coacervation across a Broad Range of Charge Densities. *Macromolecules* **2021**, *54* (14), 6878−6890.

(4) Johnson, N. R.; Wang, Y. Coacervate Delivery Systems for Proteins and Small Molecule Drugs. *Expert Opin. Drug Delivery* **2014**, *11* (12), 1829−1832.

(5) Lankalapalli, S.; Kolapalli, V. R. M. Polyelectrolyte Complexes: A Review of Their Applicability in Drug Delivery Technology. *Indian J. Pharm. Sci.* **2009**, *71* (5), 481−487.

(6) Kim, H. J.; Yang, B.; Park, T. Y.; Lim, S.; Cha, H. J. Complex Coacervates Based on Recombinant Mussel Adhesive Proteins: Their Characterization and Applications. *Soft Matter* **2017**, *13* (42), 7704−7716.

(7) Stewart, R. J.; Wang, C. S.; Shao, H. Complex Coacervates as a Foundation for Synthetic Underwater Adhesives. *Adv. Colloid Interface Sci.* **2011**, *167* (1−2), 85−93.

(8) Danielsen, S. P. O.; Nguyen, T.-Q.; Fredrickson, G. H.; Segalman, R. A. Complexation of a Conjugated Polyelectrolyte and Impact on Optoelectronic Properties. *ACS Macro Lett.* **2019**, *8* (1), 88−94.

(9) Hollingsworth, W. R.; Segura, C.; Balderrama, J.; Lopez, N.; Schleissner, P.; Ayzner, A. L. Exciton Transfer and Emergent Excitonic States in Oppositely-Charged Conjugated Polyelectrolyte Complexes. *J. Phys. Chem. B* **2016**, *120* (31), 7767−7774.

(10) Rumyantsev, A. M.; Kramarenko, E. Yu.; Borisov, O. V. Microphase Separation in Complex Coacervate Due to Incompatibility between Polyanion and Polycation. *Macromolecules* **2018**, *51* (17), 6587−6601.

(11) Smith, R. J.; Long, C. T.; Grunlan, J. C. Transparent Polyelectrolyte Complex Thin Films with Ultralow Oxygen Transmission Rate. *Langmuir* **2018**, *34* (37), 11086−11091.

(12) Petrila, L.-M.; Bucatariu, F.; Mihai, M.; Teodosiu, C. Polyelectrolyte Multilayers: An Overview on Fabrication, Properties, and Biomedical and Environmental Applications. *Materials* **2021**, *14* (15), 4152.

(13) Séon, L.; Lavalle, P.; Schaaf, P.; Boulmedais, F. Polyelectrolyte Multilayers: A Versatile Tool for Preparing Antimicrobial Coatings. *Langmuir* **2015**, *31* (47), 12856−12872.

(14) Fery, A.; Schöler, B.; Cassagneau, T.; Caruso, F. Nanoporous Thin Films Formed by Salt-Induced Structural Changes in Multilayers of Poly(Acrylic Acid) and Poly(Allylamine). *Langmuir* **2001**, *17* (13), 3779−3783.

(15) Mendelsohn, J. D.; Barrett, C. J.; Chan, V. V.; Pal, A. J.; Mayes, A. M.; Rubner, M. F. Fabrication of Microporous Thin Films from Polyelectrolyte Multilayers. *Langmuir* **2000**, *16* (11), 5017−5023.

(16) Sung, C.; Heo, Y. Porous Layer-by-Layer Films Assembled Using Polyelectrolyte Blend to Control Wetting Properties. *Polymers* **2021**, *13* (13), 2116.

(17) Schönhoff, M. Self-Assembled Polyelectrolyte Multilayers. *Curr. Opin. Colloid Interface Sci.* **2003**, *8* (1), 86−95.

(18) Wei, W.; Kim, T.-Y.; Balamurugan, A.; Sun, J.; Chen, R.; Ghosh, A.; Rodolakis, F.; McChesney, J. L.; Lakkham, A.; Evans, P. G.; Hur, S.-M.; Gopalan, P. Phase Behavior of Mixed Polymer Brushes Grown from Ultrathin Coatings. *ACS Macro Lett.* **2019**, *8* (9), 1086−1090.

(19) Müller, M. Phase Diagram of a Mixed Polymer Brush. *Phys. Rev. E: Stat., Nonlinear, Soft Matter Phys.* **2002**, *65* (3), No. 030802, DOI: 10.1103/PhysRevE.65.030802.

(20) Minko, S.; Müller, M.; Usov, D.; Scholl, A.; Froeck, C.; Stamm, M. Lateral versus Perpendicular Segregation in Mixed Polymer Brushes. *Phys. Rev. Lett.* **2002**, *88* (3), No. 035502.

(21) Price, A. D.; Hur, S.-M.; Fredrickson, G. H.; Frischknecht, A. L.; Huber, D. L. Exploring Lateral Microphase Separation in Mixed Polymer Brushes by Experiment and Self-Consistent Field Theory Simulations. *Macromolecules* **2012**, *45* (1), 510−524.

(22) Julthongpiput, D.; Lin, Y.-H.; Teng, J.; Zubarev, E. R.; Tsukruk, V. V. Y-Shaped Polymer Brushes: Nanoscale Switchable Surfaces. *Langmuir* **2003**, *19* (19), 7832−7836.

(23) Li, M.; Pester, C. W. Mixed Polymer Brushes for "Smart" Surfaces. *Polymers* **2020**, *12* (7), 1553.

(24) Lemieux, M.; Usov, D.; Minko, S.; Stamm, M.; Shulha, H.; Tsukruk, V. V. Reorganization of Binary Polymer Brushes: Reversible Switching of Surface Microstructures and Nanomechanical Properties. *Macromolecules* **2003**, *36* (19), 7244−7255.

(25) Uhlmann, P.; Ionov, L.; Houbenov, N.; Nitschke, M.; Grundke, K.; Motornov, M.; Minko, S.; Stamm, M. Surface Functionalization by Smart Coatings: Stimuli-Responsive Binary Polymer Brushes. *Prog. Org. Coat.* **2006**, *55* (2), 168−174.

(26) Santer, S.; Kopyshev, A.; Yang, H.-K.; Rühe, J. Local Composition of Nanophase-Separated Mixed Polymer Brushes. *Macromolecules* **2006**, *39* (8), 3056−3064.

(27) Uhlmann, P.; Merlitz, H.; Sommer, J.-U.; Stamm, M. Polymer Brushes for Surface Tuning. *Macromol. Rapid Commun.* **2009**, *30* (9−10), 732−740.

(28) Hur, S.-M.; Frischknecht, A. L.; Huber, D. L.; Fredrickson, G. H. Self-Consistent Field Simulations of Self- and Directed-Assembly in a Mixed Polymer Brush. *Soft Matter* **2011**, *7* (19), 8776−8788.

(29) Shusharina, N. P.; Linse, P. Oppositely Charged Polyelectrolytes Grafted onto Planar Surface: Mean-Field Lattice Theory. *Eur. Phys. J. E* **2001**, *6* (2), 147−155.

(30) Das, S.; Banik, M.; Chen, G.; Sinha, S.; Mukherjee, R. Polyelectrolyte Brushes: Theory, Modelling. *Synthesis and Applications. Soft Matter* **2015**, *11* (44), 8550−8583.

(31) Sing, C. E.; Qin, J. Bridging Field Theory and Ion Pairing in the Modeling of Polyelectrolytes and Complex Coacervation. *Macromolecules* **2023**, *56* (15), 5941−5963.

(32) Kubota, R.; Hiroi, T.; Ikuta, Y.; Liu, Y.; Hamachi, I. Visualizing Formation and Dynamics of a Three-Dimensional Sponge-like Network of a Coacervate in Real Time. *J. Am. Chem. Soc.* **2023**, *145* (33), 18316−18328.

(33) Zhao, X.; Zhang, G. A Theoretical Investigation on the pH-Induced Switching of Mixed Polyelectrolyte Brushes. *Chin. J. Polym. Sci.* **2014**, *32* (5), 568−576.

(34) Ayres, N.; Boyes, S. G.; Brittain, W. J. Stimuli-Responsive Polyelectrolyte Polymer Brushes Prepared via Atom-Transfer Radical Polymerization. *Langmuir* **2007**, *23* (1), 182−189.

(35) Yu, K.; Wang, H.; Xue, L.; Han, Y. Stimuli-Responsive Polyelectrolyte Block Copolymer Brushes Synthesized from the Si Wafer via Atom-Transfer Radical Polymerization. *Langmuir* **2007**, *23* (3), 1443−1452.

(36) Calvo, A.; Fuertes, M. C.; Yameen, B.; Williams, F. J.; Azzaroni, O.; Soler-Illia, G. J. A. A. Nanochemistry in Confined Environments: Polyelectrolyte Brush-Assisted Synthesis of Gold Nanoparticles inside Ordered Mesoporous Thin Films. *Langmuir* **2010**, *26* (8), 5559−5567.

(37) Ayres, N.; Cyrus, C. D.; Brittain, W. J. Stimuli-Responsive Surfaces Using Polyampholyte Polymer Brushes Prepared via Atom Transfer Radical Polymerization. *Langmuir* **2007**, *23* (7), 3744−3749.

(38) Sanjuan, S.; Tran, Y. Stimuli-Responsive Interfaces Using Random Polyampholyte Brushes. *Macromolecules* **2008**, *41* (22), 8721−8728.

(39) Debais, G.; Tagliazucchi, M. Microphase Separation and Aggregate Self-Assembly in Brushes of Oppositely Charged Polyelectrolytes Triggered by Ion Pairing. *J. Chem. Phys.* **2020**, *153* (14), 144903.

(40) Drechsler, A.; Elmahdy, M. M.; Uhlmann, P.; Stamm, M. pH and Salt Response of Mixed Brushes Made of Oppositely Charged Polyelectrolytes Studied by in Situ AFM Force Measurements and Imaging. *Langmuir* **2018**, *34* (16), 4739−4749.

(41) Houbenov, N.; Minko, S.; Stamm, M. Mixed Polyelectrolyte Brush from Oppositely Charged Polymers for Switching of Surface Charge and Composition in Aqueous Environment. *Macromolecules* **2003**, *36* (16), 5897−5901.

(42) Hinrichs, K.; Aulich, D.; Ionov, L.; Esser, N.; Eichhorn, K.-J.; Motornov, M.; Stamm, M.; Minko, S. Chemical and Structural Changes in a pH-Responsive Mixed Polyelectrolyte Brush Studied by Infrared Ellipsometry. *Langmuir* **2009**, *25* (18), 10987−10991.

(43) Olivier, A.; Meyer, F.; Raquez, J.-M.; Damman, P.; Dubois, P. Surface-Initiated Controlled Polymerization as a Convenient Method for Designing Functional Polymer Brushes: From Self-Assembled Monolayers to Patterned Surfaces. *Prog. Polym. Sci.* **2012**, *37* (1), 157−181.

(44) Ding, Z.; Chen, C.; Yu, Y.; de Beer, S. Synthetic Strategies to Enhance the Long-Term Stability of Polymer Brush Coatings. *J. Mater. Chem. B* **2022**, *10* (14), 2430−2443.

(45) Wei, W.; Balamurugan, A.; Dwyer, J. H.; Gopalan, P. Substrate-Independent Approach to Dense Cleavable Polymer Brushes by Nitroxide-Mediated Polymerization. *ACS Macro Lett.* **2018**, *7* (1), 100−104.

(46) Sweat, D. P.; Kim, M.; Yu, X.; Gopalan, P. A Single-Component Inimer Containing Cross-Linkable Ultrathin Polymer Coating for Dense Polymer Brush Growth. *Langmuir* **2013**, *29* (11), 3805−3812.

(47) Smith, J. D.; Salas, L. A. P.; Kreft, C.; Hur, S.-M.; Gopalan, P. Chain End-Functionalized Dense Polymer Brushes from an Inimer Coating by SI-RAFT. *Langmuir* **2023**, *39*, 8267.

(48) Chen, R.; Ayyakkalai, B.; Sun, J.; Lee, G. A.; Gopalan, P. Formamide Based Monomer for Highly Functionalized Polymers. *J. Polym. Sci.* **2022**, *60* (1), 131−141.

(49) Chen, R.; Smith, J. D.; Osores, N. N.; Gopalan, P. Synthesis and Applications of a Y-Inimer with Two Orthogonal Controlled Free Radical Polymerization Initiators. *J. Polym. Sci.* **2023**, *61* (24), 3295−3306.

(50) Husseman, M.; Malmström, E. E.; McNamara, M.; Mate, M.; Mecerreyes, D.; Benoit, D. G.; Hedrick, J. L.; Mansky, P.; Huang, E.; Russell, T. P.; Hawker, C. J. Controlled Synthesis of Polymer Brushes by "Living" Free Radical Polymerization Techniques. *Macromolecules* **1999**, *32* (5), 1424−1431.

(51) Koylu, D.; Carter, K. R. Stimuli-Responsive Surfaces Utilizing Cleavable Polymer Brush Layers. *Macromolecules* **2009**, *42* (22), 8655−8660.

(52) Petton, L.; Ciolino, A. E.; Dervaux, B.; Du Prez, F. E. From One-Pot Stabilisation to in Situ Functionalisation in Nitroxide Mediated Polymerisation: An Efficient Extension towards Atom

https://doi.org/10.1021/acs.langmuir.4c00556
Langmuir XXXX, XXX, XXX−XXX

Transfer Radical Polymerisation. *Polym. Chem.* **2012**, *3* (7), 1867−1878.

(53) Pattanayek, S. K.; Pham, T. T.; Pereira, G. G. Morphological Structures Formed by Grafted Polymers in Poor Solvents. *J. Chem. Phys.* **2005**, *122* (21), 214908.

(54) Briggs, N. P.; Budd, P. M.; Price, C.; Robb, I. D. The Synthesis and Solution Properties of Statistical and Block Copolymers of 2-Vinyl Pyridine and Acrylic Acid. *Eur. Polym. J.* **1992**, *28* (7), 739−745.

(55) Hojat, N.; Gentile, P.; Ferreira, A. M.; Šiller, L. Automatic Pore Size Measurements from Scanning Electron Microscopy Images of Porous Scaffolds. *J. Porous Mater.* **2023**, *30* (1), 93−101.

(56) AlMarzooqi, F. A.; Bilad, M. R.; Mansoor, B.; Arafat, H. A. A Comparative Study of Image Analysis and Porometry Techniques for Characterization of Porous Membranes. *J. Mater. Sci.* **2016**, *51* (4), 2017−2032.

(57) Shen, R.; Xiong, W.; Lang, X.; Wang, L.; Guo, H.; Zhou, H.; Zhang, X.; Yang, H. Quantitative Analysis of Nano-Scale Pore Structures of Broad Sense Shale Oil Reservoirs Using Atomic Force Microscopy. *Energy Explor. Exploit.* **2021**, *39* (6), 1839−1856.

(58) Zhao, S.; Li, Y.; Wang, Y.; Ma, Z.; Huang, X. Quantitative Study on Coal and Shale Pore Structure and Surface Roughness Based on Atomic Force Microscopy and Image Processing. *Fuel* **2019**, *244*, 78−90.

(59) Khanukaeva, D. Yu.; Filippov, A. N.; Bildyukevich, A. V. An AFM Study of Ultrafiltration Membranes: Peculiarities of Pore Size Distribution. *Pet. Chem.* **2014**, *54* (7), 498−506.

(60) Hur, S.-M.; Frischknecht, A. L.; Huber, D. L.; Fredrickson, G. H. Self-Assembly in a Mixed Polymer Brush with Inhomogeneous Grafting Density Composition. *Soft Matter* **2013**, *9* (22), 5341−5354.

https://doi.org/10.1021/acs.langmuir.4c00556
Langmuir XXXX, XXX, XXX−XXX